PHOTONICS INSIGHTS

Classical and generalized geometric phase in electromagnetic metasurfaces

Yinghui Guo,[a,b,c] Mingbo Pu,[a,b,c,*] Fei Zhang,[a,b,c] Mingfeng Xu,[a,b,c] Xiong Li,[a,c] Xiaoliang Ma,[a,c] and Xiangang Luo[a,c,*]
[a]State Key Laboratory of Optical Technologies on Nano-Fabrication and Micro-Engineering, Institute of Optics and Electronics, Chinese Academy of Sciences, Chengdu, China
[b]Research Center on Vector Optical Fields, Institute of Optics and Electronics, Chinese Academy of Sciences, Chengdu, China
[c]School of Optoelectronics, University of Chinese Academy of Sciences, Beijing, China

Abstract. The geometric phase concept has profound implications in many branches of physics, from condensed matter physics to quantum systems. Although geometric phase has a long research history, novel theories, devices, and applications are constantly emerging with developments going down to the subwavelength scale. Specifically, as one of the main approaches to implement gradient phase modulation along a thin interface, geometric phase metasurfaces composed of spatially rotated subwavelength artificial structures have been utilized to construct various thin and planar meta-devices. In this paper, we first give a simple overview of the development of geometric phase in optics. Then, we focus on recent advances in continuously shaped geometric phase metasurfaces, geometric–dynamic composite phase metasurfaces, and nonlinear and high-order linear Pancharatnam–Berry phase metasurfaces. Finally, conclusions and outlooks for future developments are presented.

Keywords: geometric phase; Pancharatnam–Berry phase; metasurface.

Received Apr. 26, 2022; revised manuscript received Jun. 19, 2022; accepted Jul. 4, 2022; published online Aug. 18, 2022.

[DOI: 10.3788/PI.2022.R03]

1 Introduction

In optics and electromagnetics, the geometric phase originates from the spin–orbit interaction (SOI) of light and describes the relationship between phase change and polarization conversion when light is transmitted or reflected through an anisotropic medium[1]. The general form of the geometric phase was developed by Berry in 1984[2]. He found that when a quantum system in an eigenstate is slowly transported around a circuit C by varying parameters R in its Hamiltonian $H(R)$, it will acquire a geometrical phase factor $\exp(i\gamma C)$. Since the pioneering work of Berry, the geometric phase has been applied in various fields of physics and expanded the understanding of state evolutions in different parameter spaces. The most common formulations of the geometric phase are known as the Aharonov–Bohm (AB) phase for electrons and the Pancharatnam–Berry (PB) phase for photons. Figure 1(a) shows a representative case of the AB effect. When a charged particle passes around a long solenoid, the wave function experiences a phase shift as a result of the enclosed magnetic field, despite the magnetic field being negligible in the region through which the particle passes and the particle's wave function being negligible inside the solenoid[3]. Subsequently, Chiao *et al.* considered the manifestations of this phase factor for a photon in a state of adiabatically invariant helicity, and an effective optical activity for a helical optical fiber was predicted[4]. In 1987, Aharonov and Anandan noted that the appearance of the geometric phase did not necessarily go through an adiabatic process, and the geometric phase factor can be defined for any cyclic evolution of a quantum system[5]. Another important manifestation of the geometric phase in solids is known as the Zak phase[6], which underlies the existence of protected edge states.

In 1956, Pancharatnam noticed a phase shift arising when the polarization of a photonic beam was varied in a cyclic manner, when he studied the interference between optical waves of different polarizations[7]. As illustrated in Fig. 1(b), the polarization state of the wave and its evolution can be described as a point and its trajectory on the surface of a Poincaré sphere. For the cyclic evolution of polarization displayed in Fig. 1(c), the trajectory of polarization on the Poincaré sphere is a closed curve. In this case, Pancharatnam's phase equals half the solid angle

*Address all correspondence to Mingbo Pu, pmb@ioe.ac.cn; Xiangang Luo, lxg@ioe.ac.cn

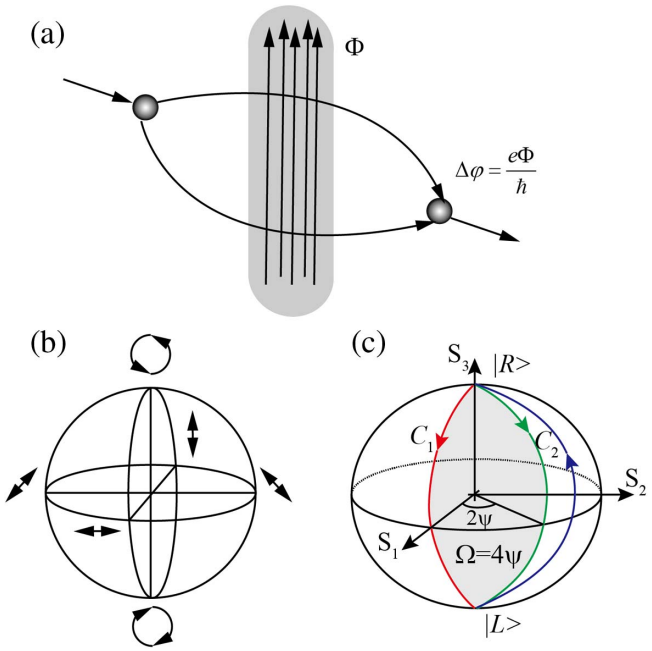

Fig. 1 (a) Schematic illustration of AB effect, where an electron encircles a magnetic flux Φ confined to a thin, long solenoid. Although the magnetic field is zero in the vicinity of the superposed wave packets, the vector potential is non-zero outside the solenoid. Thus, the electronic wave packets acquire relative phases of exp($ie\Phi/\hbar$), causing their interference patterns to change. (b) Polarization state representation on Poincaré sphere. (c) PB phase on Poincaré sphere, which equals half the solid angle (Ω) subtended at the origin by the area enclosed by the closed curves (C_1 and C_2) on the Poincaré sphere.

(Ω) subtended at the origin by the area enclosed by the closed curves (C_1 and C_2) on the Poincaré sphere. The 1/2 factor corresponds to the well-known "half-speed" rotations of spinors seen in experiments with neutrons, since it is an SU(2) transformation[8,9]. Although Pancharatnam's phase was proposed before the publication of Berry's paper, it was not noted for many years. Subsequently, Berry demonstrated the equivalence between Pancharatnam's geometric phase in polarization and the broader phenomenon of the acquired phase in the adiabatic evolution of a state in quantum mechanics[10]. Therefore, such phases are always referred to as PB phases. During the past few years, the PB phase was further extended to nonlinear PB phase and high-order linear PB phase, which will be discussed in the following sections. A simple roadmap of the development of the geometric phase is displayed in Fig. 2. Note that geometric phase is exploited to provide an additional π phase shift, excepting the circuit resonance induced phase in Ref. [11]. Several excellent reviews on geometric phases are helpful to grasp this research field from different perspectives[12-16].

2 Geometric Phases in Spatially Rotated Anisotropic Elements

In an earlier experiment, the polarization of a uniformly polarized beam was altered by a series of space-invariant (transversely homogeneous) wave plates and polarizers, and the phase difference was introduced through the evolution of the beam in the time domain. For example, as early as 1947, metallic waveguides featuring birefringent propagation with rotatable half-wave plates were sandwiched between two quarter-wave plates to generate adjustable phase shifts in phased antenna arrays for radar applications[17], as indicated in Fig. 3(a). A similar approach was independently proposed by Pancharatnam in 1955 to construct an achromatic elliptic polarizer[18]. It was not until 2001 that Hasman *et al.* considered the PB phase in the space domain[19] by using space-variant (transversely inhomogeneous) metal stripe subwavelength gratings. They demonstrated that the conversion of circular polarization was accomplished by a space-variant phase shift, which can be illustrated in a Jones matrix[20]. Specifically, a wave plate with a space-variant fast axis can be described by a coordinate dependent matrix:

$$T(r,\varphi) = \cos\left(\frac{\delta}{2}\right)\begin{pmatrix}1 & 0\\ 0 & 1\end{pmatrix} + i\sin\frac{\delta}{2}\begin{pmatrix}\cos(2\alpha) & \sin(2\alpha)\\ \sin(2\alpha) & -\cos(2\alpha)\end{pmatrix}, \tag{1}$$

where δ is the retardation phase of the wave plate, and α is the angle formed between the fast axis and the x axis. For circularly polarized incidence $E_{\text{in}}(r,\varphi) = E_0(r,\varphi)\cdot(1, i\delta)^T$, the output beam can be expressed as

$$E_{\text{out}}(r,\varphi) = T(r,\varphi)E_{\text{in}}(r,\varphi) = E_0\cos\left(\frac{\delta}{2}\right)\begin{pmatrix}1\\ i\sigma\end{pmatrix} + iE_0\sin\left(\frac{\delta}{2}\right)\exp(i2\sigma\alpha)\begin{pmatrix}1\\ -i\sigma\end{pmatrix}. \tag{2}$$

Equation (2) shows that after passing the space-variant anisotropic wave plates, a circularly polarized beam is primarily scattered into waves of the same polarization as that of the incident beam without a phase change and waves of the opposite circular polarization with a spin-dependent phase change $\Phi = 2\sigma\alpha$. Here, $\sigma = \pm 1$ represents left- and right-handed circular polarization (LCP and RCP), respectively. Obviously, by controlling the local orientation of the fast axes of the wave plate elements between zero and π, one can realize phase variation that covers the full zero to 2π range while maintaining equal transmission amplitude. Note that the amplitudes of opposite circular polarization depend on the phase retardation δ [i.e., $\sin(\delta/2)$], and a wave plate with phase retardation of π is desired to realize 100% conversion efficiency. For artificial wave plates based on subwavelength structures, the operation band is limited due to resonant dispersion. Therefore, dispersion engineering technology has been proposed to construct broadband wave plates[21,22].

Subsequently, a series of PB phase optical elements, composed of space-variant large pixel-sized periodic gratings or annular grooves [Fig. 3(b)], was developed for beam deflection, helical beam generation, and coronagraphs[20,23-25]. As shown in Figs. 3(c) and 3(d), with the development of advanced fabrication technology, e.g., laser direct writing, electron beam lithography, and focused ion beams, the building blocks of space-variant PB phase optical elements were generally dominated by subwavelength plasmonic[26-31] or dielectric elements[32-37], wherein the corresponding metasurfaces were referred to as geometric phase metasurfaces. Owing to the abrupt phase that changes over the scale of the wavelength, the propagation behavior of light can be manipulated arbitrarily. The metasurface-assisted law of refraction and reflection (MLRR)[38], a kind of generalized law of reflection and refraction[11], and broadband

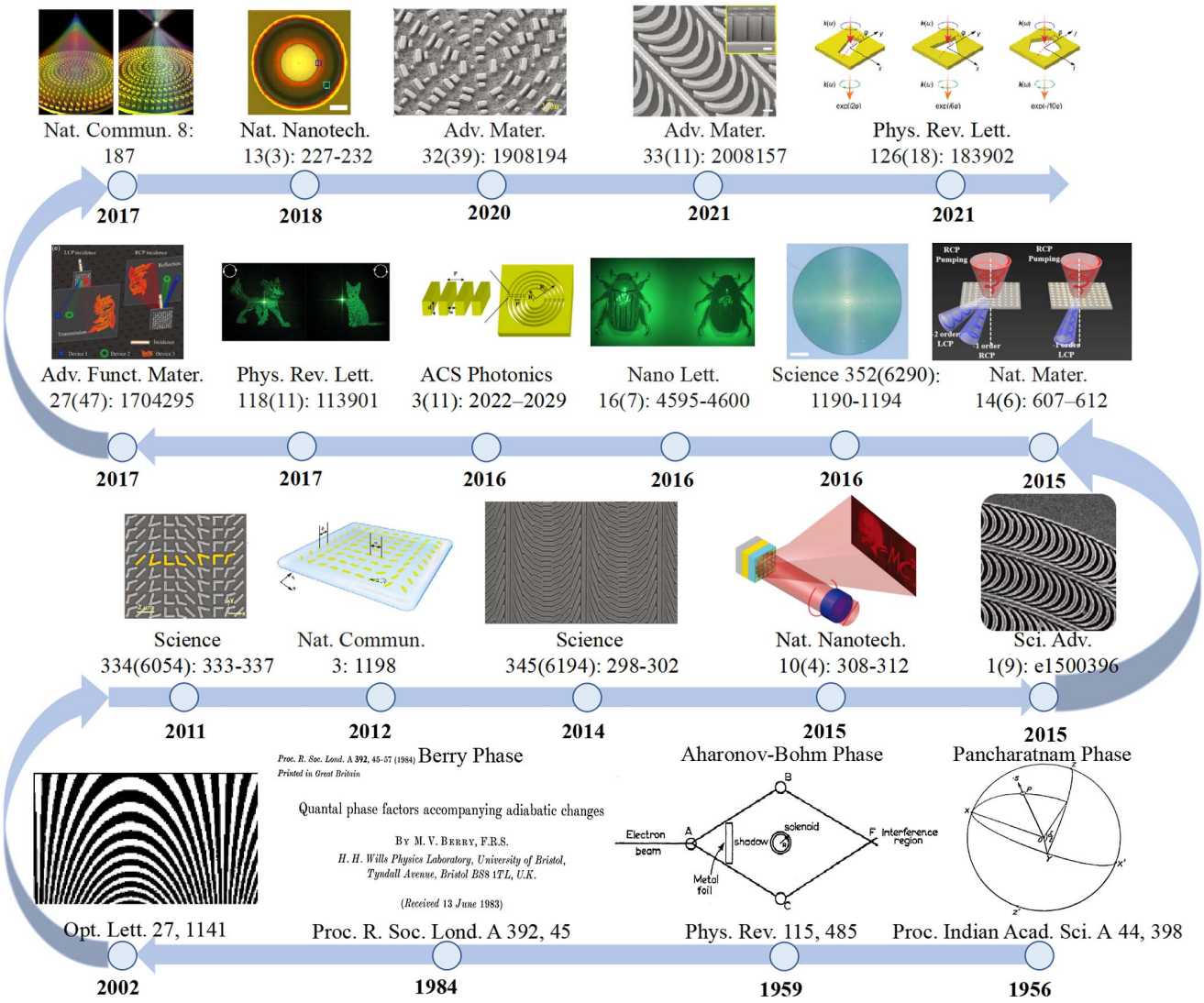

Fig. 2 Roadmap of the development of the geometric phase in optics.

sub-diffraction focusing and imaging[26,39] have been demonstrated. Metasurfaces find widespread applications in planar lenses[40-42], the photonic spin Hall effect (PSHE)[43,44], directional coupling[45], holographic imaging[46-53], beam generation[30,54-56], and beam steering antennas[57]. For example, by matching the geometric phases of nano-slots on silver to specific superimpositions of the inward and outward surface plasmon profiles for the two spins, arbitrary spin-dependent orbitals can be generated in a slot-free region[58]. In addition to the traditional design approach, heuristic design methodology has been adopted in nanophotonics to improve the design efficiency and device performances[59].

3 From Discrete Geometric Phase Metasurface to Continuous Counterparts

Geometric phase metasurfaces are generally composed of multiple discrete meta-atoms, which inevitably degrade the overall performance of metasurfaces, for example, decreasing the diffraction efficiency of metasurfaces and the purity of generated orbit angular momentum (OAM)[60]. During the past few years, quasi-continuous geometric phase metasurfaces composed of catenaries[30], concentric rings[60], sinusoidal metallic strip arrays[61], free-shaped meander lines[62,63], and other shaped structures[32,64-68] have been utilized to overcome the shortfalls above, as indicated in Fig. 4. All these proposals have demonstrated that continuous metasurfaces possess higher efficiency or broader bandwidths than their discrete counterparts owing to the elimination of resonance. Interestingly, the continuous and linear phase shift covering $[0, 2\pi]$ can be imparted by a single optical catenary[30,43], i.e., the so-called "catenary of equal phase gradient." Consequently, perfect OAM and even high-order non-diffraction Bessel beams can be generated by arranging the catenaries in various forms, as shown in Fig. 4(a). As a branch of subwavelength optics, catenary optics include not only catenary shaped quasi-continuous structures, but also catenary fields and catenary dispersion. The former is generated by the coupling of evanescent waves, with typical applications in super-resolution imaging and lithography. The latter provides a general guideline for realizing the quick design of functional metasurfaces, such as broadband electromagnetic absorbers and flat antennas. Readers may refer to Ref. [69] for a comprehensive review.

Subsequently, it has been demonstrated that the metamorphosis of an optical catenary, either metallic or dielectric, can

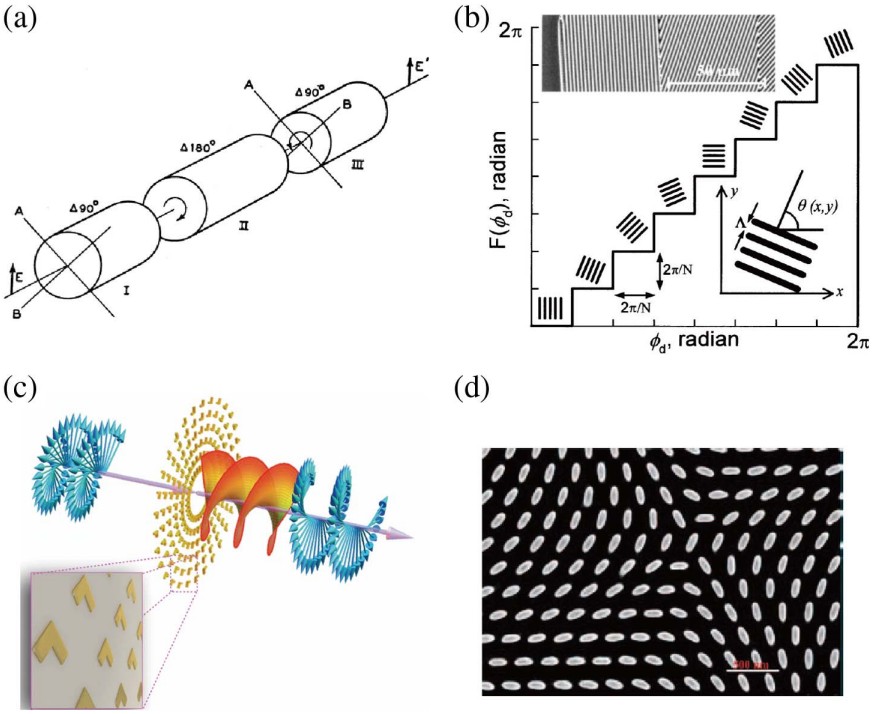

Fig. 3 Different elements for generating PB phase. (a) An adjustable waveguide phase shift at the microwave band is composed of a rotatable half-wave plate sandwiched between two quarter-wave plates. Reproduced with permission from Ref. [17]. (b) Actual quantized phase as a function of the desired phase, as well as discrete local grating orientation, with a scanning electron microscope (SEM) image of space-variant gratings displayed in the inset. Reproduced with permission from Ref. [25]. (c) Schematic representation of geometric phase metasurface for generating OAMs via PB phase. Reproduced with permission from Ref. [27]. (d) SEM image of geometric phase metasurface composed of space-variant plasmonic nano-apertures. Scale bar represents 500 nm. Reproduced with permission from Ref. [29].

be utilized to generate a quadratic phase profile for wide-field-of-view (FOV) imaging[70,71] and beam steering[57] as well as a cubic phase profile for accelerating beam generation[72,73], as displayed in Figs. 4(b) and 4(c). According to the principle of geometric phase, a novel metasurface design methodology by integrating the predefined phase function of space-variant stripes can be extended for arbitrary phase profiles[62,71]. To cancel the propagation phase modulation, the geometries of dielectric catenaries are tailored elaborately. Subsequently, Wang *et al.* proposed dielectric nanoarc structures as building blocks that support different electromagnetic resonant modes at localized areas. These dielectric nanoarcs have the distinct advantage of a continuous-phase gradient along the curved trajectory within an individual building block[64]. By combining with the principle of a chiral-detour phase, complex holograms with high efficiency were achieved.

4 Merging PB Phase and Propagation Phase for Spin-Decoupling Modulation

For a common geometric phase metasurface, geometric phase is generated accompanied by spin conversion and phase modulation conjugating with each other when the spin state of incidence is reversed, which is inconvenient in practical applications. For example, for a focusing metalens composed of a geometric phase metasurface, it can operate only under a specific spin state and will become divergent for other spin states[74]. In addition, holographic images will be centrosymmetric with each other under different spin states[50], which means no additional information is imparted.

To break the conjugate symmetry of a geometric phase metasurface under opposite helicity illumination, Guo *et al.* proposed to merge it with a polarization-independent propagation phase into a single metasurface[60]. Due to the spin independence of the dynamical propagation phase in the surface plasmon polariton (SPP) wave, the total phases for two spin states are decoupled. The composite phase modulation method has been implemented by dielectric nanopillars with spatially variant orientations and geometric parameters. Two research teams independently demonstrated the spin-decoupled holographic imaging and OAM generation in 2017[75-78], and the concept of spin-decoupled metasurfaces has been further expanded from circular polarization to arbitrary orthogonal polarizations.

Besides phase decoupling modulation, amplitude decoupling modulation[76,79,80] has also been demonstrated via two or multiple meta-atom metasurfaces. By adjusting the orientations and geometric parameters of meta-atoms in the supercell, the LCP and RCP components satisfy different interference conditions. As a consequence, one can make one component be transmitted and the other be reflected. By rotating the super unit cell following the PB phase principle, different functionalities, e.g., deflection, OAM generation, and holographic imaging,

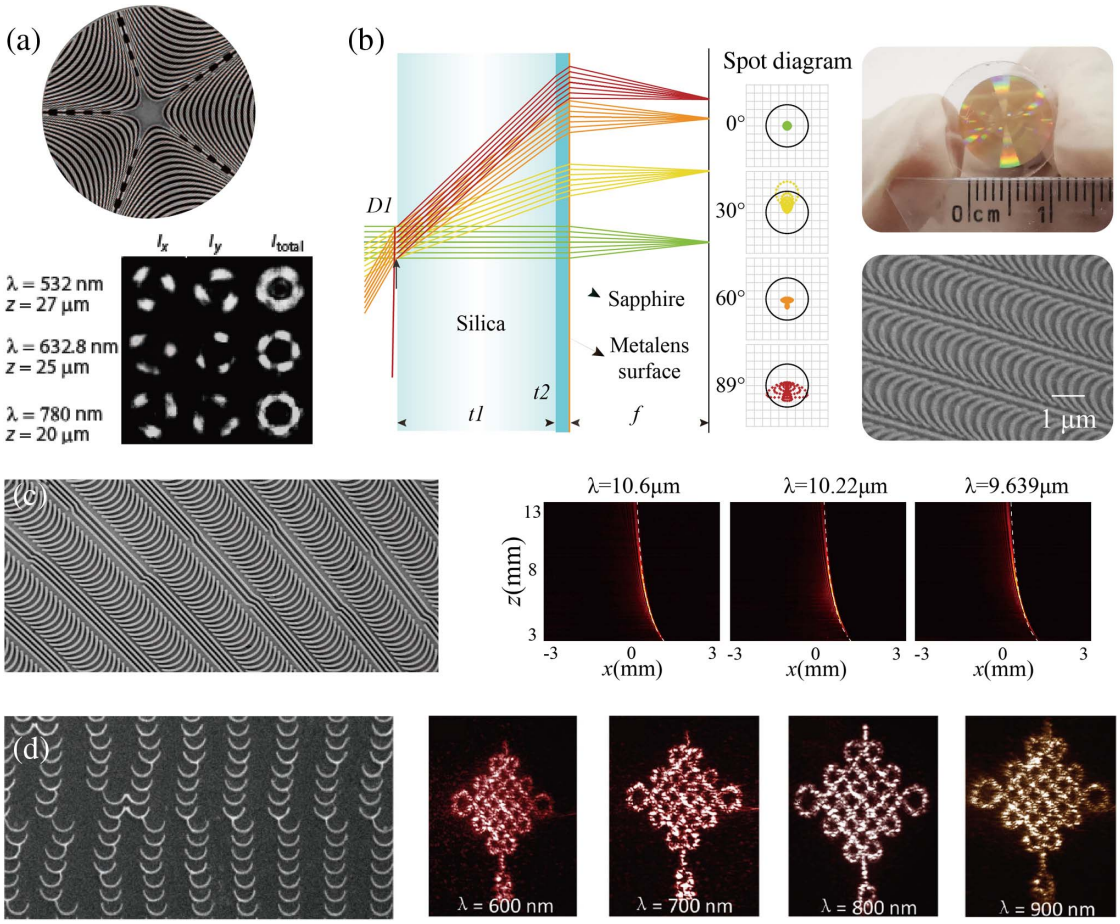

Fig. 4 Quasi-continuous geometric phase. (a) SEM figure of the rotational optical catenary array and measured intensity patterns of OAMs generated through PB phase. Reproduced with permission from Ref. [30]. (b) Optical layout of wide-FOV camera with a single layer quadratic phase metalens. Optical and SEM images of fabricated wide-angle metalens composed of catenary-like structures. Reproduced with permission from Ref. [71]. (c) SEM image of cubic phase metasurface composed of catenary-like structures and measured results of the generated accelerating beams. Reproduced with permission from Ref. [73]. (d) SEM image of holographic metasurface composed of C-shaped dielectric nanoarcs and corresponding holographic images at different wavelengths. Reproduced with permission from Ref. [64].

have been demonstrated[76]. Following a similar methodology, decoupling amplitude modulation has been expanded to orthogonal linear polarizations and arbitrary orthogonal polarizations[80]. Subsequently, more degrees of freedom (DOFs) are introduced to realize more independent channels. For example, a chirality-assisted phase can decouple two co-polarized outputs, and thus be an alternative solution for designing arbitrary modulated-phase metasurfaces with distinct wavefront manipulation in all four output channels[81]. Recently, by combining four nanoblocks in one pixel, optical elements with five DOFs and printing-hologram functionalities with six DOFs of the Jones matrix have been experimentally demonstrated[82].

Since two orthogonal spin states can be independently manipulated with different phase shifts, vectorial optical beams can be generated more conveniently and compactly[83-87]. Liu *et al.* have proposed and experimentally demonstrated the broadband generation of perfect Poincaré beams via a single-layer dielectric metasurface for visible light[88]. With the spatial superposition of two perfect optical vortices, different perfect Poincaré beams, whose total angular momenta are described by the hybrid-order Poincaré sphere, can be generated. More recently, a longitudinally varied vector field was experimentally demonstrated by a monolayer metasurface[86], as shown in Figs. 5(a) and 5(b), which are distinct from traditional elements that manipulate polarization in a single transverse plane. The underlying mechanism relies on transforming an incident waveform into an ensemble of pencil-like beams with different polarization states that beat along the optical axis, thereby changing the resulting polarization at will, locally, as light propagates. Subsequently, a simultaneous transversally and longitudinally varied vector optical field (VOF) has been further demonstrated by decoupling two orthogonal polarization states through asymmetric photonic SOIs to obtain custom-tailored phase and amplitude differences between opposite components and then coherently synthesize them in three-dimensional space. As illustrated in Fig. 5, the polarization distribution switches continuously and periodically between radial and azimuthal polarizations[89]. Furthermore, the vector field can be dynamically

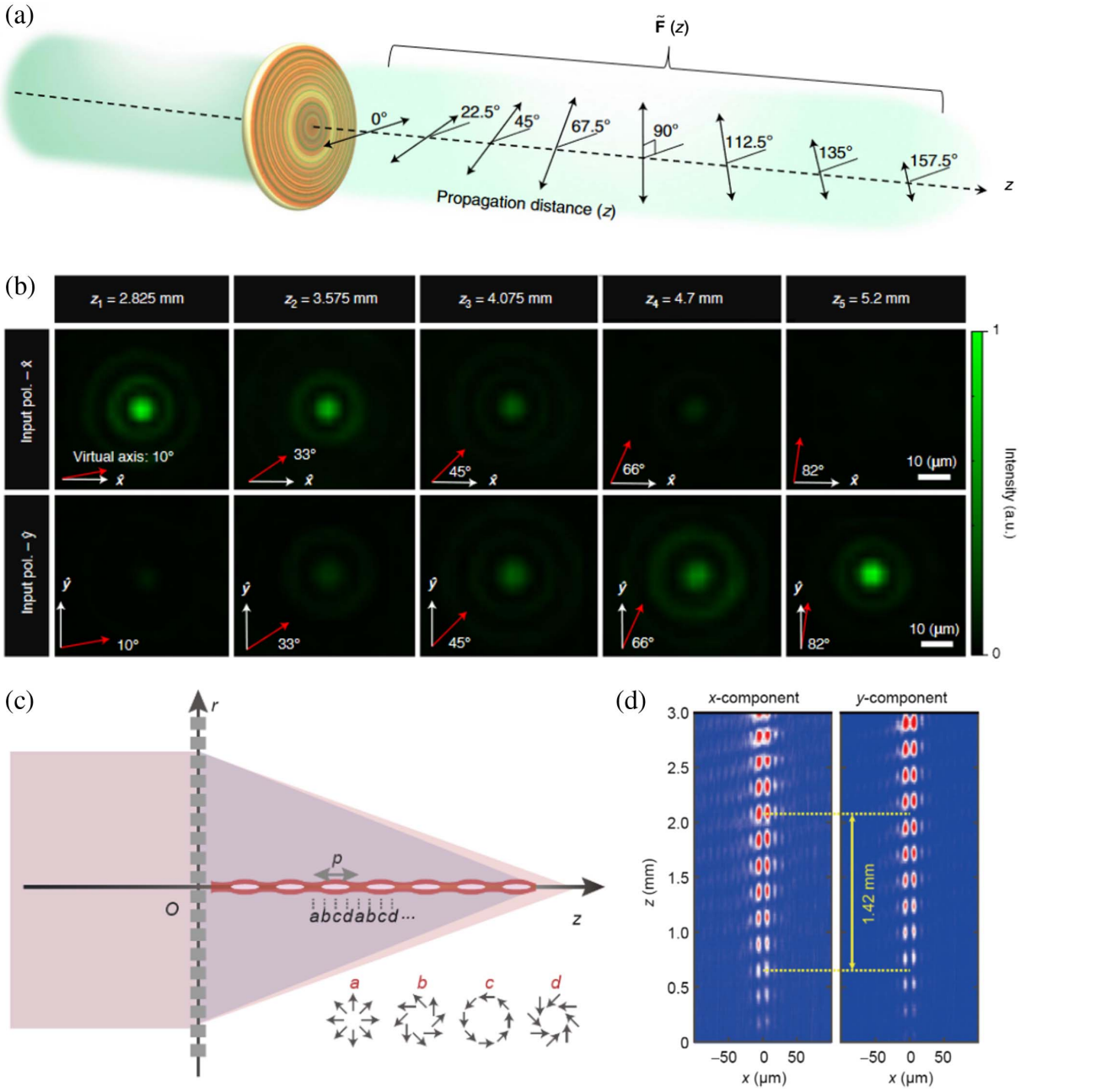

Fig. 5 (a) Schematic of a *z*-dependent polarizing device (polarizer or retarder) that enables variable polarization operations to be performed at different *z* planes along the optical path. (b) Measured transverse profiles of the output beam at different planes along the propagation direction for *x* and *y* incident polarizations. White arrows depict incident polarization (in the *xy* plane), and red arrows represent the state of polarization analyzed at each *z* plane. Reproduced with permission from Ref. [86]. Three-dimensional synthetic VOF generated by a monolayer composite phase metasurface: (c) schematic diagram; (d) measured intensity pattern of orthogonal linear polarizations. Black arrows depict the virtual principal axis orientation of the polarizing element at each *z* plane. Reproduced with permission from Ref. [89].

tuned by rotating the incident polarization state. This work extends polarization optics from two-dimensional space to 3D space, allowing the arbitrary generation and manipulation of 3D VOFs with temporal tunability.

Considering the principle of reciprocity, VOF generators may also be used to characterize and detect VOFs through spin–orbit coupling effects[90,91]. It has been demonstrated that a single angular metalens with an azimuthal-quadratic phase profile can simultaneously determine the phase and polarization singularities of a cylindrical vortex vector beam (CVVB) via spin-dependent photonic momentum transformation[92]. As shown in Fig. 6, CVVBs with phase and polarization

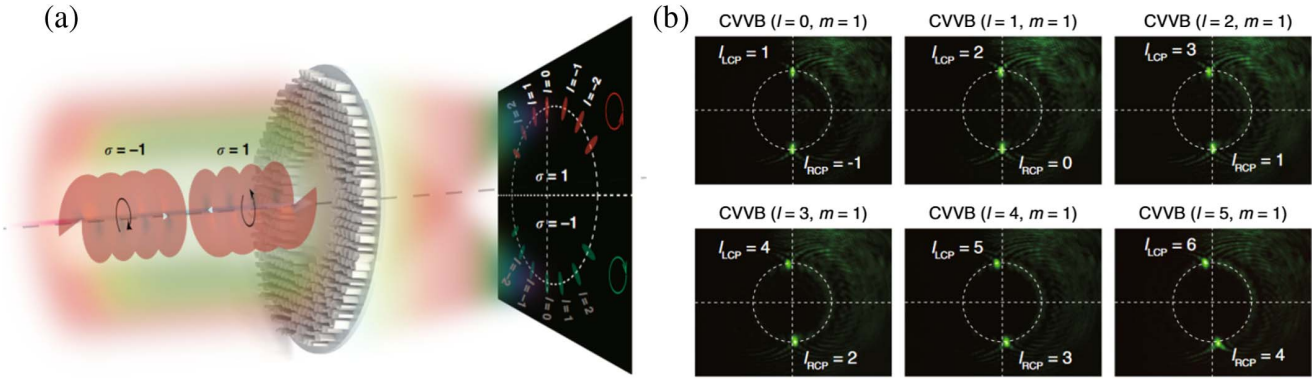

Fig. 6 Single spin-decoupled metasurface for vectorial optical field characterization. (a) Schematic diagram. (b) Measured intensity pattern of CVVB with different intensity patterns. CVVB, cylindrical vortex vector beam. Reproduced with permission from Ref. [92].

singularities can be treated as a superimposition of an LCP vortex with topological charge $l + m$ and an RCP vortex with topological charge $l - m$, which are separated into top and bottom half-screens, with their azimuthal angles proportional to the topological charge. Luo's group has proposed and investigated the concept of asymmetric photonic SOI since 2017, and interesting applications can be found in recent reviews[93,94].

5 PB Phase in the Nonlinear Regime

In 2015, the concept of PB phase optical elements was extended to the nonlinear regime. Three research groups independently reported the nonlinear PB phase in metasurfaces nearly at the same time[95-97]. It was found that under the illumination of a circularly polarized fundamental wave, transmitted nonlinear harmonic waves with the same or opposite helicity will carry phase factors of $(n-1)\sigma\varphi$ or $(n+1)\sigma\varphi$, respectively, where n is the order of harmonic generation[96]. To satisfy the selection rules for the harmonic generation of circularly polarized fundamental waves, a single nanostructure with m-fold rotational symmetry allows only harmonic orders of $n = lm \pm 1$, where l is an integer, and the "+" and "−" signs correspond to harmonic generation of the same and opposite circular polarization, respectively. For example, for a nanorod structure with two-fold rotational symmetry (C2), third-harmonic generation (THG) signals with both the same and opposite circular polarizations to that of the fundamental wave can be generated, and the corresponding spin-dependent phases of $2\sigma\theta$ and $4\sigma\theta$ are generated. On the contrary, the THG process is not allowed for a nanostructure with four-fold rotational symmetry (C4) for the same polarization state as the incident polarization, as revealed by Fig. 7(a). Hence, only a single THG signal with a geometric phase of $4\sigma\theta$ for opposite circular polarization is generated. Furthermore, the impact of rotational symmetry on THG for circularly polarized light in nonlinear plasmonic crystals has also been investigated, which may inspire the design of novel spin-dependent nonlinear plasmonic devices[98,99]. Such a nonlinear geometric phase was further confirmed through THG signal deflection via a gradient metasurface, as shown in Figs. 7(b) and 7(c). A similar phenomenon was reported in Ref. [95] via multiquantum-well-based nonlinear plasmonic metasurfaces, as indicated in Figs. 7(d) and 7(e). Readers may refer to a recent review for comprehensive details[100]. Subsequently, Li *et al.* demonstrated the existence of a nonlinear geometric Berry phase in the four-wave mixing process, which was applied to spin-controlled nonlinear light generation from plasmonic metasurfaces[101]. The polarization state of four-wave mixing from ultrathin metasurfaces, comprising gold meta-atoms with four-fold rotational symmetry, can be controlled by manipulating the spin of the excitation beams. The mutual orientation of the meta-atoms in the metasurface influences the intensity of four-wave mixing via the geometric phase effects.

By exploiting the concept of the PB phase in the nonlinear optical regime, many interesting functional devices such as nonlinear lenses[102-104], nonlinear encryption[105], and nonlinear imaging[106,107], have been proposed. The multidimensional nonlinear polarization response of nano-material was achieved in a single heterodyne measurement by active manipulation of the polarization states of incident light[108], and a new kind of metasurface-based THz emitter with the polarization and phase of THz waves finely controlled was demonstrated[109]. By exploiting linear and nonlinear geometric phases simultaneously as different channels, spin and wavelength multiplexed nonlinear metasurface holography provides independent, nondispersive, and crosstalk-free post-selective channels for holographic multiplexing and multidimensional optical data storage, anti-counterfeiting, and optical encryption[110].

6 High-Order Linear PB Phase

In principle, all previous methods to generate a linear PB phase rely on the polarization conversion enabled by anisotropic structures, and subwavelength structures with ≥ 3 rotational symmetries are thought to be isotropic and no linear geometric phase can be observed[100,111]. In 2021, Xie *et al.* demonstrated that subwavelength structures with rotational symmetries ≥ 3 can tailor optical anisotropy, and high-order linear geometric phases that manifest as multiple times the rotation angle of the meta-atoms can be achieved[112]. The anisotropy is attributed to the lattice coupling effect when the symmetries of the meta-atom and lattice are incompatible. The high-order geometric phase can be understood by analyzing the rotation dependence of meta-atoms and their effective principal axes. As shown in Fig. 8, for meta-atoms with one-fold (C1) or two-fold (C2) rotational symmetry, the principal axis has a rotation angle equal to the single meta-atom. For meta-atoms with three and higher rotational symmetry, however, there is a multiple

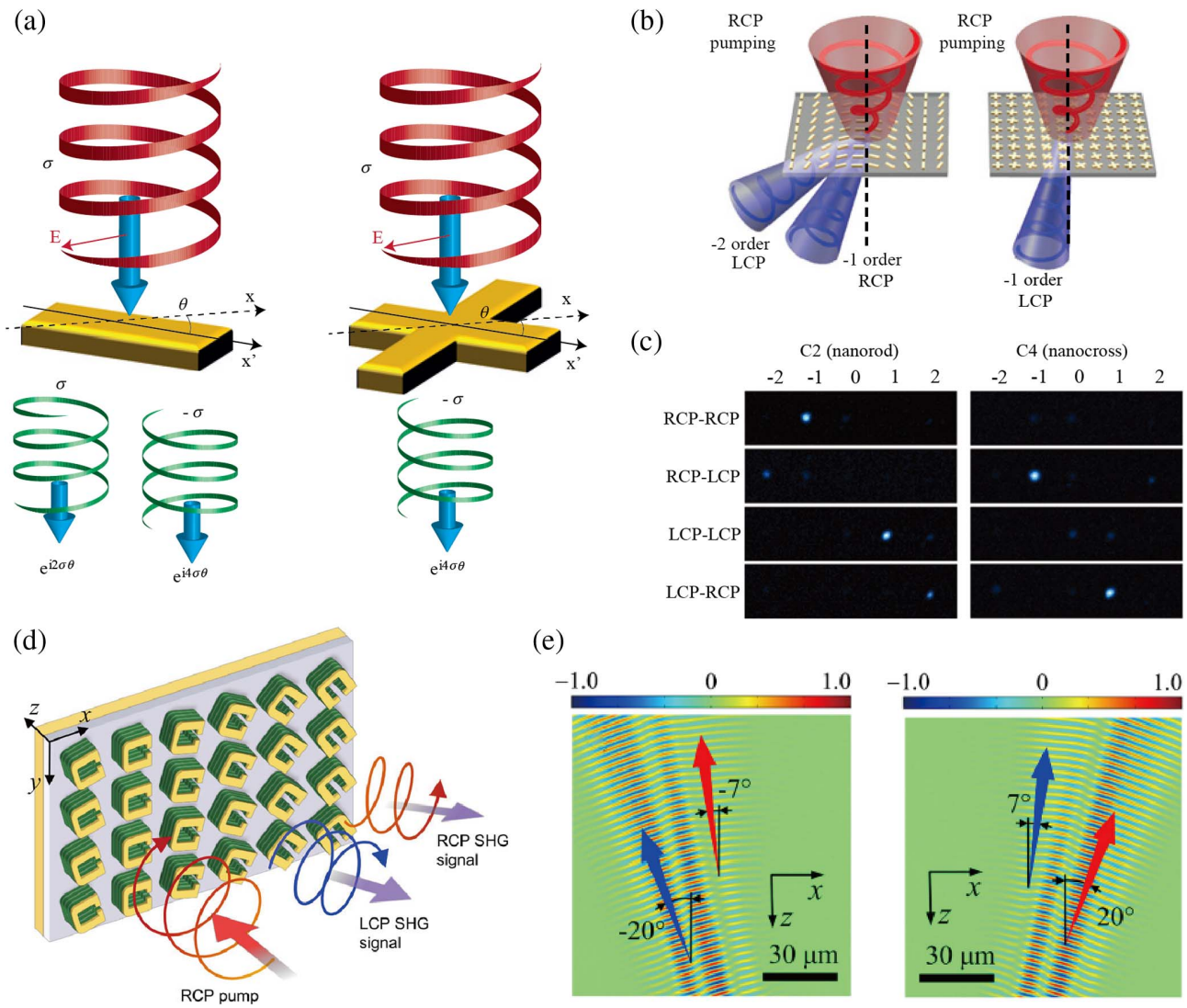

Fig. 7 Nonlinear geometric phase metasurface. (a) Nonlinear geometric phases are generated through THG of a C2 nanostructure and a C4 nanostructure. (b) Illustration of phase-controlled diffraction of THG signals for RCP light at the fundamental frequency. (c) Measured diffraction pattern of THG signals from C2 and C4 metasurfaces for circular polarization states of the fundamental and THG waves. (a)–(c) Reproduced with permission from Ref. [96]. (d) Sketch of the proposed PB nonlinear metasurface with a phase gradient in x direction. The MQW blocks are sandwiched between U-shaped gold resonators and a metallic ground plane. The incident circularly polarized wave at frequency ω generates simultaneously RCP and LCP nonlinear waves at 2ω. (e) Simulated field distributions and deflection directions of second-harmonic generation (SHG) signals of different circular polarization states. (d), (e) Reproduced with permission from Ref. [95].

and lattice-dependent relationship between the rotation angles of the principal axes and meta-atoms. For instance, for triangular meta-atoms in a square lattice, owing to their three-fold rotational symmetry, the principal axis has a rotation angle of 3φ when the meta-atoms are rotated by φ. For square meta-atoms arranged in a hexagonal lattice, when the meta-atoms are rotated by φ, the principal axis has a rotation angle of 10φ. By taking advantage of the multifold relationship, high-order geometric phases equal to multiple times the rotation angle of meta-atoms can be obtained.

After rigorous mathematical derivation, for a square lattice, the geometric phase for meta-atoms with n-fold rotational symmetry can be written as

$$\Phi = \begin{cases} \pm 2n\varphi, & n \text{ is odd} \\ \pm n\varphi, & n \text{ is even} \end{cases}. \tag{3}$$

For a hexagonal lattice, the geometric phase can be deduced with a bit more complex expression:

$$\Phi = 2 \times \frac{60^\circ}{\gamma}\varphi, \tag{4}$$

or

$$\Phi = -2 \times \frac{120^\circ}{\gamma}\varphi, \tag{5}$$

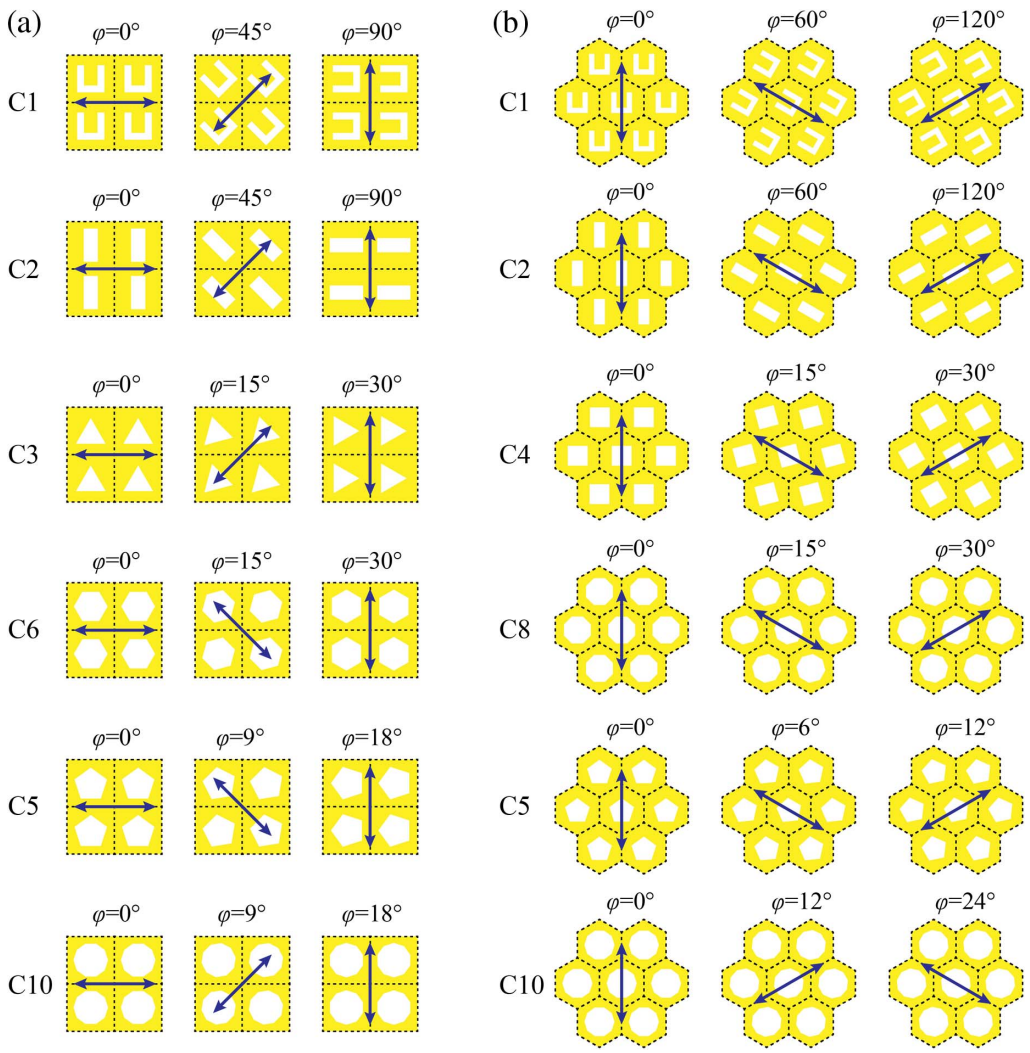

Fig. 8 High-order linear PB phase metasurfaces. (a) Rotation dependence of the principal axis and meta-atoms with C1, C2, C3, C6, C5, and C10 rotational symmetry in the square lattice. (b) Rotation dependence of the principal axis and meta-atoms with C1, C2, C4, C8, C5, and C10 rotational symmetry in the hexagonal lattice. Double-headed arrows indicate the orientations of the principal array axis.

where γ denotes the minimal rotation angle of the meta-atoms to rotate the principal axis by 60° or 120°. The choice of expression should be determined by investigating either the geometric phase or the transmission coefficients along the principal axes at different rotational angles.

The nontrivial phase shifts introduced by meta-atoms in the square or hexagonal lattice are summarized in Table 1. According to these relationships, one can obtain a well-defined geometric phase with the desired gradient in the range of 0 to 2π by choosing the appropriate rotational symmetry of meta-atoms and lattices.

7 Conclusion and Outlook

In summary, we have briefly reviewed the history of geometric phase and recent advances in geometric phase metasurfaces.

Table 1 Geometric Phases Introduced by Meta-Atoms with C1–C10 Rotational Symmetries in the Square or Hexagonal Lattice under LCP and RCP Illuminations.

Lattice	Polarization	C1	C2	C3	C4	C5	C6	C7	C8	C9	C10
Square	LCP	2φ	2φ	6φ		-10φ	-6φ	-14φ		18φ	10φ
	RCP	-2φ	-2φ	-6φ		10φ	6φ	14φ		-18φ	-10φ
Hexagonal	LCP	2φ	2φ		8φ	20φ		14φ	8φ		-10φ
	RCP	-2φ	-2φ		-8φ	-20φ		-14φ	-8φ		10φ

Compared to discrete geometric phase metasurfaces, quasi-continuous and continuous geometric phase metasurfaces exhibit great advantages such as higher efficiency and broader bandwidth. Merging geometric phase and propagation phase can break the conjugate symmetry of traditional PB phase and bring new degrees of freedom for light manipulation. For example, one can simultaneously manipulate the phase and dispersion of a transmitted light wave to realize multiple wavelength or achromatic applications[113]. As two kinds of emerging geometric phases, nonlinear PB phase and high-order linear PB phase have been discussed in detail, providing us with a new understanding of the geometric phase as well as light–matter interaction in nanophotonics. Although this paper focuses mainly on the geometric phase metasurface, the geometric phase principle is extended to liquid crystal planar devices by changing the tangential curves of the molecular orientation pattern[114], owing to the high polarization conversion efficiency and easy fabrication process. For a focusing lens, the tangential curves possess a catenary profile.

In the future, there are some interesting research directions that can be explored, for example, the combination of nonlinear geometric phase and lattice-mismatch induced high-order geometric phase, dynamic and reconfigurable modulation based on high-order geometric phase, and merging high-order PB phase with dynamic phase in a single metasurface. The idea of high-order linear PB phase can be applied to nonlinear optics and will promote new findings about nonlinear geometric phase[115], and provides new approaches for manipulations of light in nonlinear metasurfaces. Furthermore, multiple-dimensional light manipulation including polarization amplitude, polarization phase, complex amplitude, phase-dispersion engineering, and VOF[116-121] can be realized. Recently, progress in geometric phase inside a light beam at a sharp interface has provided very different geometric-phase-enabled novel phenomena distinct from those reviewed in this paper[122,123]. For example, a wave-vector-varying PB phase has been found that arises naturally in the transmission and reflection processes in homogeneous media for paraxial beams with small incident angles[124]. The eigenpolarization states of transmission and reflection processes are determined by the local wave vectors of the incident beam. A small incident angle breaks the rotational symmetry and induces a PB phase that varies linearly with the transverse wave vector, resulting in the PSHE. Additionally, an intriguing phase transition between vortex generation and spin Hall shift triggered by varying the incidence angle is revealed. After reflection/refraction of a spin-polarized light beam at sharp interfaces, the beam contains two components: normal and abnormal modes acquiring spin-redirection Berry phases and PB phases, respectively[125]. Efficiency enhancement by several-thousand times compared to that at a conventional slab was observed at a purposely designed metamaterial slab. Therefore, it is expected that the concept and connotation of generalized geometric phase will be greatly enriched. As a typical application of the geometric phase, its dispersionless property has been utilized to realize super-resolving telescopes by generating broadband super-oscillation[39], where a resolution as high as 0.64 times that of the Rayleigh criterion was observed in an experiment with a white light source. In addition, by exploiting the geometric phase, anisotropic super-resolution photolithography can be achieved via extraordinary Young's interference (EYI)[126].

Acknowledgments

This work was supported by the National Natural Science Foundation of China (61875253, 62105338, and U20A20217), National Key Research and Development Program of China (2021YFA1401000), Sichuan Science and Technology Program (2021ZYCD001), and Chinese Academy of Sciences Youth Innovation Promotion Association (2019371).

Disclosures

The authors declare no conflicts of interest.

References

1. P. K. Aravind, "A simple proof of Pancharatnam's theorem," *Opt. Commun.* **94**, 191 (1992).
2. M. V. Berry, "Quantal phase factors accompanying adiabatic changes," *Proc. R. Soc. Lond. A* **392**, 45 (1984).
3. Y. Aharonov and D. Bohm, "Significance of electromagnetic potentials in the quantum theory," *Phys. Rev.* **115**, 485 (1959).
4. R. Y. Chiao and Y.-S. Wu, "Manifestations of Berry's topological phase for the photon," *Phys. Rev. Lett.* **57**, 933 (1986).
5. Y. Aharonov and J. Anandan, "Phase change during a cyclic quantum evolution," *Phys. Rev. Lett.* **58**, 1593 (1987).
6. J. Zak, "Berry's phase for energy bands in solids," *Phys. Rev. Lett.* **62**, 2747 (1989).
7. S. Pancharatnam, "Generalized theory of interference and its applications," *Proc. Indian Acad. Sci. A* **44**, 398 (1956).
8. R. Simon, H. J. Kimble, and E. C. G. Sudarshan, "Evolving geometric phase and its dynamical manifestation as a frequency shift: an optical experiment," *Phys. Rev. Lett.* **61**, 19 (1988).
9. R. Bhandari, "SU (2) phase jumps and geometric phases," *Phys. Lett. A* **157**, 221 (1991).
10. M. V. Berry, "The adiabatic phase and Pancharatnam's phase for polarized light," *J. Mod. Opt.* **34**, 1401 (1987).
11. N. Yu et al., "Light propagation with phase discontinuities: generalized laws of reflection and refraction," *Science* **334**, 333 (2011).
12. C. P. Jisha, S. Nolte, and A. Alberucci, "Geometric phase in optics: from wavefront manipulation to waveguiding," *Laser Photonics Rev.* **15**, 2100003 (2021).
13. J. Anandan, "The geometric phase," *Nature* **360**, 307 (1992).
14. M. Berry, "Geometric phase memories," *Nat. Phys.* **6**, 148 (2010).
15. C. A. Mead, "The geometric phase in molecular systems," *Rev. Mod. Phys.* **64**, 51 (1992).
16. E. Cohen et al., "Geometric phase from Aharonov–Bohm to Pancharatnam–Berry and beyond," *Nat. Rev. Phys.* **1**, 437 (2019).
17. A. G. Fox, "An adjustable wave-guide phase changer," *Proc. IRE* **35**, 1489 (1947).
18. S. Pancharatnam, "Achromatic combinations of birefringent plates," *Proc. Indian Acad. Sci. A* **41**, 137 (1955).
19. Z. Bomzon, V. Kleiner, and E. Hasman, "Pancharatnam-Berry phase in space-variant polarization-state manipulations with subwavelength gratings," *Opt. Lett.* **26**, 1424 (2001).
20. Z. Bomzon et al., "Space-variant Pancharatnam-Berry phase optical elements with computer-generated subwavelength gratings," *Opt. Lett.* **27**, 1141 (2002).
21. Y. Guo et al., "Dispersion management of anisotropic metamirror for super-octave bandwidth polarization conversion," *Sci. Rep.* **5**, 8434 (2015).
22. M. Pu et al., "Spatially and spectrally engineered spin-orbit interaction for achromatic virtual shaping," *Sci. Rep.* **5**, 9822 (2015).
23. D. Mawet et al., "Annular groove phase mask coronagraph," *Astrophys. J.* **633**, 1191 (2005).

24. G. Biener et al., "Formation of helical beams by use of Pancharatnam-Berry phase optical elements," *Opt. Lett.* **27**, 1875 (2002).
25. E. Hasman et al., "Polarization dependent focusing lens by use of quantized Pancharatnam–Berry phase diffractive optics," *Appl. Phys. Lett.* **82**, 328 (2003).
26. D. Tang et al., "Ultrabroadband superoscillatory lens composed by plasmonic metasurfaces for subdiffraction light focusing," *Laser Photonics Rev.* **9**, 713 (2015).
27. E. Karimi et al., "Generating optical orbital angular momentum at visible wavelengths using a plasmonic metasurface," *Light Sci. Appl.* **3**, e167 (2014).
28. G. Zheng et al., "Metasurface holograms reaching 80% efficiency," *Nat. Nanotechnol.* **10**, 308 (2015).
29. X. Ma et al., "A planar chiral meta-surface for optical vortex generation and focusing," *Sci. Rep.* **5**, 10365 (2015).
30. M. Pu et al., "Catenary optics for achromatic generation of perfect optical angular momentum," *Sci. Adv.* **1**, e1500396 (2015).
31. F. Zhang et al., "Multistate switching of photonic angular momentum coupling in phase-change metadevices," *Adv. Mater.* **32**, 1908194 (2020).
32. D. Lin et al., "Dielectric gradient metasurface optical elements," *Science* **345**, 298 (2014).
33. F. Aieta et al., "Multiwavelength achromatic metasurfaces by dispersive phase compensation," *Science* **347**, 1342 (2015).
34. A. Arbabi et al., "Dielectric metasurfaces for complete control of phase and polarization with subwavelength spatial resolution and high transmission," *Nat. Nanotechnol.* **10**, 937 (2015).
35. M. Khorasaninejad et al., "Metalenses at visible wavelengths: diffraction-limited focusing and subwavelength resolution imaging," *Science* **352**, 1190 (2016).
36. F. Ding et al., "Versatile polarization generation and manipulation using dielectric metasurfaces," *Laser Photonics Rev.* **14**, 2000116 (2020).
37. M. Khorasaninejad et al., "Multispectral chiral imaging with a metalens," *Nano Lett.* **16**, 4595 (2016).
38. X. Luo, "Principles of electromagnetic waves in metasurfaces," *Sci. China Phys. Mech. Astron* **58**, 594201 (2015).
39. Z. Li et al., "Achromatic broadband super-resolution imaging by super-oscillatory metasurface," *Laser Photonics Rev.* **12**, 1800064 (2018).
40. Z. Yue et al., "Terahertz metasurface zone plates with arbitrary polarizations to a fixed polarization conversion," *Opto-Electron. Sci.* **1**, 210014 (2022).
41. X. Zang et al., "Metasurfaces for manipulating terahertz waves," *Light Adv. Manuf.* **2**, 148 (2021).
42. K. Liu et al., "Active tuning of electromagnetically induced transparency from chalcogenide-only metasurface," *Light Adv. Manuf.* **2**, 251 (2021).
43. X. Luo et al., "Broadband spin Hall effect of light in single nanoapertures," *Light Sci. Appl.* **6**, e16276 (2017).
44. X. Ling et al., "Giant photonic spin Hall effect in momentum space in a structured metamaterial with spatially varying birefringence," *Light Sci. Appl.* **4**, e290 (2015).
45. Y. Meng et al., "Optical meta-waveguides for integrated photonics and beyond," *Light Sci. Appl.* **10**, 235 (2021).
46. L. Huang et al., "Three-dimensional optical holography using a plasmonic metasurface," *Nat. Commun.* **4**, 2808 (2013).
47. X. Li et al., "Multicolor 3D meta-holography by broadband plasmonic modulation," *Sci. Adv.* **2**, e1601102 (2016).
48. G. Qu et al., "Reprogrammable meta-hologram for optical encryption," *Nat. Commun.* **11**, 5484 (2020).
49. Y. Hu et al., "Trichromatic and tripolarization-channel holography with noninterleaved dielectric metasurface," *Nano Lett.* **20**, 994 (2020).
50. D. Wen et al., "Helicity multiplexed broadband metasurface holograms," *Nat. Commun.* **6**, 8241 (2015).
51. J.-H. Park and B. Lee, "Holographic techniques for augmented reality and virtual reality near-eye displays," *Light Adv. Manuf.* **3**, 1 (2022).
52. Z.-L. Deng et al., "Multi-freedom metasurface empowered vectorial holography," *Nanophotonics* **11**, 0622 (2022).
53. H. Gao et al., "Recent advances in optical dynamic meta-holography," *Opto-Electronic Adv.* **4**, 210030 (2021).
54. Y. Ming et al., "Creating composite vortex beams with a single geometric metasurface," *Adv. Mater.* **34**, 2109714 (2022).
55. S. Zhang et al., "Generation of achromatic auto-focusing Airy beam for visible light by an all-dielectric metasurface," *J. Appl. Phys.* **131**, 043104 (2022).
56. Q. Zhou et al., "Generation of perfect vortex beams by dielectric geometric metasurface for visible light," *Laser Photon. Rev.* **15**, 2100390 (2021).
57. Y. Guo et al., "High-efficiency and wide-angle beam steering based on catenary optical fields in ultrathin metalens," *Adv. Opt. Mater.* **6**, 1800592 (2018).
58. S. Xiao et al., "Flexible coherent control of plasmonic spin-Hall effect," *Nat. Commun.* **6**, 8360 (2015).
59. T. Ma et al., "Benchmarking deep learning-based models on nanophotonic inverse design problems," *Opto-Electron. Sci.* **1**, 210012 (2022).
60. Y. Guo et al., "Merging geometric phase and plasmon retardation phase in continuously shaped metasurfaces for arbitrary orbital angular momentum generation," *ACS Photonics* **3**, 2022 (2016).
61. Y. Guo et al., "Scattering engineering in continuously shaped metasurface: an approach for electromagnetic illusion," *Sci. Rep.* **6**, 30154 (2016).
62. X. Zhang et al., "A quasi-continuous all-dielectric metasurface for broadband and high-efficiency holographic images," *J. Phys. D* **53**, 465105 (2020).
63. X. Zhang et al., "Ultra-broadband metasurface holography via quasi-continuous nano-slits," *J. Phys. D* **53**, 104002 (2019).
64. D. Wang et al., "Broadband high-efficiency chiral splitters and holograms from dielectric nanoarc metasurfaces," *Small* **15**, 1900483 (2019).
65. D. Hakobyan et al., "Tailoring orbital angular momentum of light in the visible domain with metallic metasurfaces," *Adv. Opt. Mater.* **4**, 306 (2016).
66. M. Xu et al., "Topology-optimized catenary-like metasurface for wide-angle and high-efficiency deflection: from a discrete to continuous geometric phase," *Opt. Express* **29**, 10181 (2021).
67. Z. Gong et al., "Broadband efficient vortex beam generation with metallic helix array," *Appl. Phys. Lett.* **113**, 071104 (2018).
68. D. Hakobyan et al., "Tailoring orbital angular momentum of light in the visible domain with metallic metasurfaces," *Adv. Opt. Mater.* **4**, 306 (2015).
69. X. Luo et al., "Catenary functions meet electromagnetic waves: opportunities and promises," *Adv. Opt. Mater.* **8**, 2001194 (2020).
70. M. Pu et al., "Nanoapertures with ordered rotations: symmetry transformation and wide-angle flat lensing," *Opt. Express* **25**, 31471 (2017).
71. F. Zhang et al., "Extreme-angle silicon infrared optics enabled by streamlined surfaces," *Adv. Mater.* **33**, 2008157 (2021).
72. Y. Guo et al., "Polarization-controlled broadband accelerating beams generation by single catenary-shaped metasurface," *Adv. Opt. Mater.* **7**, 1900503 (2019).
73. F. Zhang et al., "Broadband and high-efficiency accelerating beam generation by dielectric catenary metasurfaces," *Nanophotonics* **9**, 20200057 (2020).
74. X. Chen et al., "Dual-polarity plasmonic metalens for visible light," *Nat. Commun.* **3**, 1198 (2012).
75. F. Zhang et al., "Symmetry breaking of photonic spin-orbit interactions in metasurfaces," *Opto-Electron. Eng.* **44**, 319 (2017).
76. F. Zhang et al., "All-dielectric metasurfaces for simultaneous giant circular asymmetric transmission and wavefront shaping

based on asymmetric photonic spin–orbit interactions," *Adv. Fun. Mater.* **27**, 1704295 (2017).
77. J. P. B. Mueller et al., "Metasurface polarization optics: independent phase control of arbitrary orthogonal states of polarization," *Phys. Rev. Lett.* **118**, 113901 (2017).
78. R. C. Devlin et al., "Arbitrary spin-to-orbital angular momentum conversion of light," *Science* **358**, 896 (2017).
79. J. Cai et al., "Simultaneous polarization filtering and wavefront shaping enabled by localized polarization-selective interference," *Sci. Rep.* **10**, 14477 (2020).
80. Q. Fan et al., "Independent amplitude control of arbitrary orthogonal states of polarization via dielectric metasurfaces," *Phys. Rev. Lett.* **125**, 267402 (2020).
81. Y. Yuan et al., "Independent phase modulation for quadruplex polarization channels enabled by chirality-assisted geometric-phase metasurfaces," *Nat. Commun.* **11**, 4186 (2020).
82. Y. Bao et al., "Toward the capacity limit of 2D planar Jones matrix with a single-layer metasurface," *Sci. Adv.* **7**, eabh0365 (2021).
83. D. Wang et al., "Efficient generation of complex vectorial optical fields with metasurfaces," *Light Sci. Appl.* **10**, 67 (2021).
84. D. Wang et al., "High-efficiency metadevices for bifunctional generations of vectorial optical fields," *Nanophotonics* **10**, 685 (2021).
85. I. Kim et al., "Pixelated bifunctional metasurface-driven dynamic vectorial holographic color prints for photonic security platform," *Nat. Commun.* **12**, 3614 (2021).
86. A. H. Dorrah et al., "Metasurface optics for on-demand polarization transformations along the optical path," *Nat. Photonics* **15**, 287 (2021).
87. N. A. Rubin et al., "Jones matrix holography with metasurfaces," *Sci. Adv.* **7**, eabg7488 (2021).
88. M. Liu et al., "Broadband generation of perfect Poincaré beams via dielectric spin-multiplexed metasurface," *Nat. Commun.* **12**, 2230 (2021).
89. F. Zhang et al., "Synthetic vector optical fields with spatial and temporal tenability," *Sci. China Phys. Mech. Astron.* **65**, 254211 (2022).
90. J. Ni et al., "Multidimensional phase singularities in nanophotonics," *Science* **374**, eabj0039 (2021).
91. S. Zhang et al., "Broadband detection of multiple spin and orbital angular momenta via dielectric metasurface," *Laser Photonics Rev.* **14**, 2000062 (2020).
92. Y. Guo et al., "Spin-decoupled metasurface for simultaneous detection of spin and orbital angular momenta via momentum transformation," *Light Sci. Appl.* **10**, 63 (2021).
93. X. Luo et al., "Symmetric and asymmetric photonic spin-orbit interaction in metasurfaces," *Prog. Quant. Electron.* **79**, 100344 (2021).
94. Z. Fei et al., "Metasurfaces enabled by asymmetric photonic spin-orbit interactions," *Opto-Electron Eng.* **47**, 200366 (2020).
95. M. Tymchenko et al., "Gradient nonlinear Pancharatnam-Berry metasurfaces," *Phys. Rev. Lett.* **115**, 207403 (2015).
96. G. Li et al., "Continuous control of the nonlinearity phase for harmonic generations," *Nat. Mater.* **14**, 607 (2015).
97. N. Segal et al., "Controlling light with metamaterial-based nonlinear photonic crystals," *Nat. Photonics* **9**, 180 (2015).
98. S. Chen et al., "Symmetry-selective third-harmonic generation from plasmonic metacrystals," *Phys. Rev. Lett.* **113**, 033901 (2014).
99. K. Konishi et al., "Polarization-controlled circular second-harmonic generation from metal hole arrays with threefold rotational symmetry," *Phys. Rev. Lett.* **112**, 135502 (2014).
100. G. Li, S. Zhang, and T. Zentgraf, "Nonlinear photonic metasurfaces," *Nat. Rev. Mater.* **2**, 17010 (2017).
101. G. Li et al., "Spin and geometric phase control four-wave mixing from metasurfaces," *Laser Photon. Rev.* **12**, 1800034 (2018).
102. M. Ma et al., "Optical information multiplexing with nonlinear coding metasurfaces," *Laser Photon. Rev.* **13**, 1900045 (2019).
103. Z. Li et al., "Multiplexed nondiffracting nonlinear metasurfaces," *Adv. Funct. Mater.* **30**, 1910744 (2020).
104. C. Schlickriede et al., "Imaging through nonlinear metalens using second harmonic generation," *Adv. Mater.* **30**, 1703843 (2018).
105. F. Walter et al., "Ultrathin nonlinear metasurface for optical image encoding," *Nano Lett.* **17**, 3171 (2017).
106. B. Reineke et al., "Silicon metasurfaces for third harmonic geometric phase manipulation and multiplexed holography," *Nano Lett.* **19**, 6585 (2019).
107. W. Zhao et al., "Chirality-selected second-harmonic holography with phase and binary amplitude manipulation," *Nanoscale* **12**, 13330 (2020).
108. Z. Gao et al., "Reconstruction of multidimensional nonlinear polarization response of Pancharatnam-Berry metasurfaces," *Phys. Rev. B* **104**, 054303 (2021).
109. C. McDonnell et al., "Functional THz emitters based on Pancharatnam-Berry phase nonlinear metasurfaces," *Nat. Commun.* **12**, 30 (2021).
110. W. Ye et al., "Spin and wavelength multiplexed nonlinear metasurface holography," *Nat. Commun.* **7**, 11930 (2016).
111. M. A. Kats et al., "Giant birefringence in optical antenna arrays with widely tailorable optical anisotropy," *Proc. Nat. Acad. Sci.* **109**, 12364 (2012).
112. X. Xie et al., "Generalizd Pancharatnam-Berry phase in rotationally symmetric meta-atoms," *Phys. Rev. Lett.* **126**, 3902 (2021).
113. S. Yijia et al., "Achromatic metalens based on coordinative modulation of propagation phase and geometric phase," *Opto-Electron Eng.* **47**, 200237 (2020).
114. N. V. Tabiryan et al., "Advances in transparent planar optics: enabling large aperture, ultrathin lenses," *Adv. Opt. Mater.* **9**, 2001692 (2021).
115. Y. Tang et al., "Nonlinear vectorial metasurface for optical encryption," *Phys. Rev. Appl.* **12**, 024028 (2019).
116. Y. Zhang et al., "Multidimensional manipulation of wave fields based on artificial microstructures," *Opto-Electron. Adv.* **3**, 200002 (2020).
117. Y. Wang, Q. Fan, and T. Xu, "Design of high efficiency achromatic metalens with large operation bandwidth using bilayer architecture," *Opto-Electron. Adv.* **4**, 200008 (2021).
118. R. Zhao et al., "Multichannel vectorial holographic display and encryption," *Light Sci. Appl.* **7**, 95 (2018).
119. E. Arbabi et al., "Vectorial holograms with a dielectric metasurface: ultimate polarization pattern generation," *ACS Photonics* **6**, 2712 (2019).
120. L. Fang et al., "Vectorial doppler metrology," *Nat. Commun.* **12**, 4186 (2021).
121. E. Wang et al., "Complete control of multichannel, angle-multiplexed, and arbitrary spatially varying polarization fields," *Adv. Opt. Mater.* **8**, 1901674 (2020).
122. J. Wang et al., "Shifting beams at normal incidence via controlling momentum-space geometric phases," *Nat. Commun.* **12**, 6046 (2021).
123. Z. Zhang et al., "Enhancing the efficiency of the topological phase transitions in spin–orbit photonics," *Appl. Phys. Lett.* **120**, 181102 (2022).
124. W. Zhu et al., "Wave-vector-varying Pancharatnam-Berry phase photonic spin hall effect," *Phys. Rev. Lett.* **126**, 083901 (2021).
125. X. Ling et al., "Topology-induced phase transitions in spin-orbit photonics," *Laser Photon. Rev.* **15**, 2000492 (2021).
126. M. Pu et al., "Revisitation of extraordinary Young's interference: from catenary optical fields to spin-orbit interaction in metasurfaces," *ACS Photonics* **5**, 3198 (2018).